Observation of the $\Sigma_c(2800)$ isotriplet and the latest measurements of $\Lambda_c(2625)^+$ by the Belle Collaboration – contents analysis

Kerim Guseynov

Based on arXiv:hep-ex/0412069
arXiv:2212.04062

Faculty of Physics
Moscow State University

Dec 20, 2022

Introduction

- Charm baryon resonances provide crucial tests for phenomenological theories.
- Their masses, widths are always beneficial.
- Decay channels are especially valuable.
- $\Lambda_c(2625)^+$ has long been under investigation.
- $\Lambda_c(2625)^+$ has a very small width. Predictions range from 0.01 to 0.5 MeV.
- Its decay channels have never been measured, either.

Belle detector

Located at KEKB at KEK (High Energy Accelerator Research Organization, Japan)

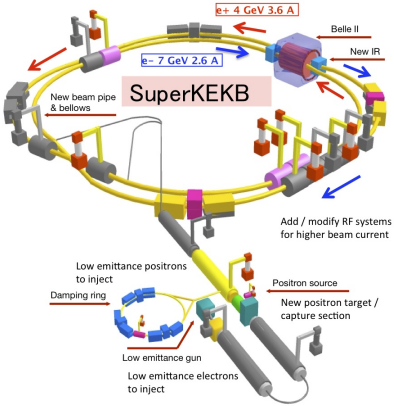

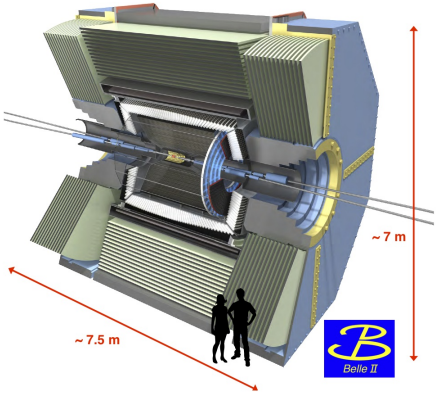

Vertex detector

Drift chamber

Cherenkov detector

Time-of-flight counters

Scintillator

ee annihilation at $\Upsilon(4S)$

Data selection for $\Sigma_c(2800)$ observation

Σ_c^* resonances are observed in the $\Lambda_c^+\pi^{-,+,0}$ spectra.

- Λ_c^+ are reconstructed in $\Lambda_c^+ \to pK^-\pi^+$
- Particle identification is based on the drift chamber, time-of-flight sensors and Cherenkov detectors.
- PID efficiency is 83% for protons, 84% for kaons, 90% for pions.
- PID cuts reduce background to 3%, 13%, 53%, respectively.
- Λ_c^+ mass is limited to within 1.6σ of the known value.
- π^0 are reconstructed as two electromagnetic showers with an inv. mass within 1.6σ of m_{π^0}.
- $\Lambda_c^+\pi$ must carry 70% or more of the full ee collision energy.
- Kinematic cut on the direction of the π relative to $\Lambda_c^+\pi$ boost reduces soft pion background.

$\Delta M(\Lambda_c^+\pi) = M(\Lambda_c^+\pi) - M(\Lambda_c^+)$ spectra: an issue

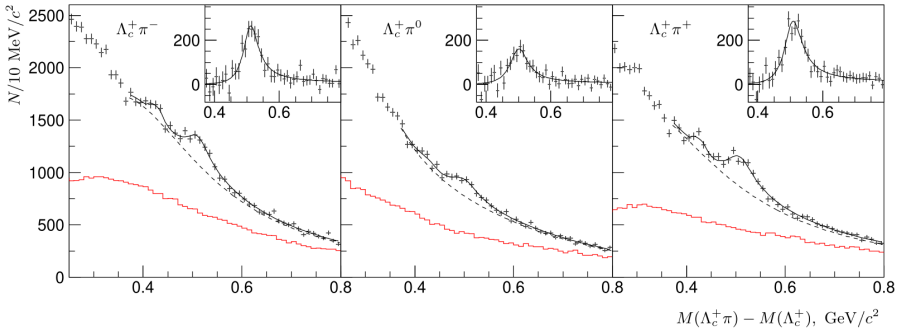

FIG. 1: $M(\Lambda_c^+\pi) - M(\Lambda_c^+)$ distributions of the selected $\Lambda_c^+\pi^-$ (left), $\Lambda_c^+\pi^0$ (middle) and $\Lambda_c^+\pi^+$ (right) combinations. Data from the Λ_c^+ signal window (points with error bars) and normalized sidebands (histograms) are shown, together with the fits described in the text (solid curves) and their combinatorial background components (dashed). The insets show the background subtracted distributions in the signal region (points with error bars) with the signal component from the fit superimposed.

No features in sidebands

$\Lambda_c(2880)^+$ contribution: from MC

$\Lambda_c(2880)^+ \to \Sigma_c\pi$ component in the $\Lambda_c^+\pi$ spectra

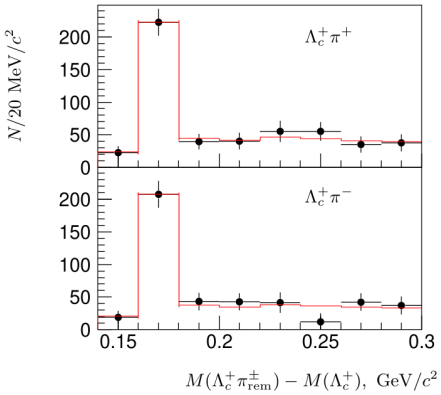

FIG. 2: Yield of $\Lambda_c(2880)^+$ *vs.* $\Delta M(\Lambda_c^+\pi^+_{\rm rem})$ (top) and $\Delta M(\Lambda_c^+\pi^-_{\rm rem})$ (bottom). The peaks are due to intermediate $\Sigma_c(2455)^{++}$ and $\Sigma_c(2455)^0$ states, respectively, in $\Lambda_c(2880)^+$ decay: see the text.

$\Lambda_c(2880)^+$ contribution to $\Lambda_c^+\pi$:

Shape is taken from the MC.

Yield is also fixed in the $\Lambda_c^+\pi$ fits.

It is taken from $\Lambda_c^+\pi^+\pi^-$ fits in bins of $\Lambda_c^+\pi$.

30% of events proceed via $\Sigma_c(2455)$.

For $\Lambda_c^+\pi^0$, yield is based on isospin arithmetic.

$\Delta M(\Lambda_c^+\pi) = M(\Lambda_c^+\pi) - M(\Lambda_c^+)$ spectra and fits

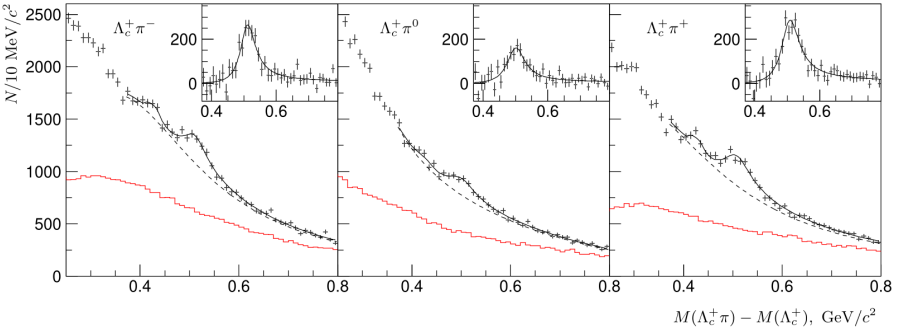

FIG. 1: $M(\Lambda_c^+\pi) - M(\Lambda_c^+)$ distributions of the selected $\Lambda_c^+\pi^-$ (left), $\Lambda_c^+\pi^0$ (middle) and $\Lambda_c^+\pi^+$ (right) combinations. Data from the Λ_c^+ signal window (points with error bars) and normalized sidebands (histograms) are shown, together with the fits described in the text (solid curves) and their combinatorial background components (dashed). The insets show the background subtracted distributions in the signal region (points with error bars) with the signal component from the fit superimposed.

D-wave Breit-Wigner conv. with resolution $\Lambda_c(2880)^+$ contribution

3rd order inverse polynomial comb. bkg.

Systematic uncertainties of $\Sigma_c(2800)$

- S-wave or P-wave Breit-Wigner for $\Sigma_c(2800)$.
- Extend fitting interval to the left.
- Comb. background model:
  - Normal polynomials
  - Higher and lower order inverse polynomials
  - Modulated exponents
  - These plus normalized Λ_c^+ sidebands.
- Vary normalization of $\Lambda_c(2880)^+$ component within 2σ.
- Vary momentum scale cut.
- Vary kinematic cut on π angle.

Dominant contributions: fitting range and bkg. model.

Checks for $\Sigma_c(2800)$

- Similar structures observed in other Λ_c^+ modes:
  - $\Lambda_c^+ \to pK_S^0$
  - $\Lambda_c^+ \to \Lambda^0\pi^+$
- Not reflections of higher resonances in $\Lambda_c^+\pi\pi$: these spectra exhibit no features.

Efficiencies of $\Sigma_c(2800)$ measurement

- Kinematic cut on π direction:
  P-parity is conserved in strong decays.
  $\Lambda_c^+\pi$ fits performed with kin. cuts complementary to the excluded region.
  Corrected for detection efficiency.
- Momentum scale cut:
  $\Sigma_c(2800)$ yields in bins of x_p.
  x_p spectra are extrapolated.

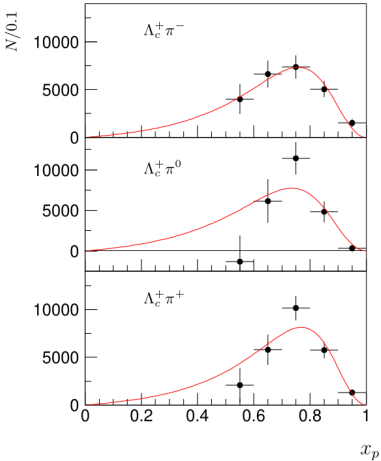

FIG. 3: Spectra of scaled momentum x_p for $\Sigma_c(2800)^0$ (top), for $\Sigma_c(2800)^+$ (middle) and for $\Sigma_c(2800)^{++}$ (bottom) states.

$\Sigma_c(2800)$ measurement results

TABLE I: Signal yield, mass and width for $\Sigma_c(2800)^0$, $\Sigma_c(2800)^+$ and $\Sigma_c(2800)^{++}$. The first uncertainty is statistical, the second one is systematic.

State	Yield $/10^3$	ΔM, MeV$/c^2$	Γ, MeV
$\Sigma_c(2800)^0$	$2.24^{+0.79+1.03}_{-0.55-0.50}$	$515.4^{+3.2+2.1}_{-3.1-6.0}$	61^{+18+22}_{-13-13}
$\Sigma_c(2800)^+$	$1.54^{+1.05+1.40}_{-0.57-0.88}$	$505.4^{+5.8+12.4}_{-4.6-\ 2.0}$	62^{+37+52}_{-23-38}
$\Sigma_c(2800)^{++}$	$2.81^{+0.82+0.71}_{-0.60-0.49}$	$514.5^{+3.4+2.8}_{-3.1-4.9}$	75^{+18+12}_{-13-11}

$$\sigma(ee \to \Sigma_c(2800)X) \times \mathcal{B}(\Sigma_c(2800) \to \Lambda_c^+\pi^+) = \begin{array}{ll} (2.04^{+0.72+0.97}_{-0.50-0.52} \pm 0.53)\ \text{pb} & \text{for } \Sigma_c(2800)^0 \\ (2.6^{+1.8+2.4}_{-1.0-1.5} \pm 0.7)\ \text{pb} & \text{for } \Sigma_c(2800)^+ \\ (2.36^{+0.69+0.64}_{-0.50-0.47} \pm 0.61)\ \text{pb} & \text{for } \Sigma_c(2800)^{++} \end{array}$$

Data selection for $\Lambda_c(2625)^+$ measurement

- $\Lambda_c(2625)^+$ is reconstructed in $\Lambda_c(2625)^+ \to \Lambda_c^+ \pi^+ \pi^-$.
- Λ_c^+ is reconstructed in $pK^-\pi^+$.
- p, K, and π are selected based on likelihood fits.
- Each of them must be 60% to 40% or better compared with alternative hypotheses.
- PID cuts efficiency:
  87% for protons, 84% for kaons, 96% for pions.
- Λ_c^+ mass must be within 1.6σ of the known value.
- $\Lambda_c(2625)^+$ must carry 70% or more of the full ee collision enegry.
- Additional exp. and MC data for $D^{*+} \to D^0\pi^+$, $D^0 \to K^-\pi^+$ for mass resolution.

Mass resolution of D^{*+} decays

- These decays are very similar kinematically.
- $M(D^0\pi) - M(D^0)$ fit with a Breit-Wigner conv. with a double Gaussian function.
- Breit-Wigner width is fixed to the world average.
- Without track smearing, $\sigma^{\text{exp}}_{\text{reso}}/\sigma^{\text{MC}}_{\text{reso}} = 114\%$
- With track smearing, $\sigma^{\text{exp}}_{\text{reso}}/\sigma^{\text{MC}}_{\text{reso}} = 86\%$

$\Lambda_c^+\pi^+\pi^-$ fit with $\Lambda_c(2625)^+$

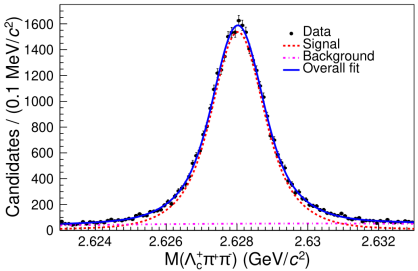

FIG. 1: Distribution of the invariant mass $M(\Lambda_c^+\pi^+\pi^-)$ where the Λ_c^+ mass is fixed to the PDG value. The solid line shows the overall distribution and the dashed lines show the individual signal and background components.

Signal is a Breit-Wigner
conv. with a double Gaussian.
Bkg. is a 2nd order polynomial.

Resolution:

Without smearing, scaled by 114%:
0.490 ± 0.025 MeV width

With smearing, scaled by 86%:
0.293 ± 0.026 MeV width

With smearing, not scaled: zero natural width

Only an upper limit: $\Gamma(\Lambda_c(2625)^+) < 0.52$ MeV

Overview of Dalitz plot fit

- Amplitude is the sum of 5 $\Lambda_c(2625)^+$ decay channels:
  $\Sigma_c(2455)^0$, $\Sigma_c(2520)^0$, $\Sigma_c(2455)^{++}$, $\Sigma_c(2520)^{++}$, $\Lambda_c^+\pi^+\pi^-$.
- Bkg. described by a constant amplitude.
  Different from 3-body $\Lambda_c^+\pi^+\pi^-$ since the bkg. is flat across the Dalitz plot.
- Masses and widths of $\Sigma_c^{(*)}$ are constrained to the their world averages.

Dalitz plot in the signal region

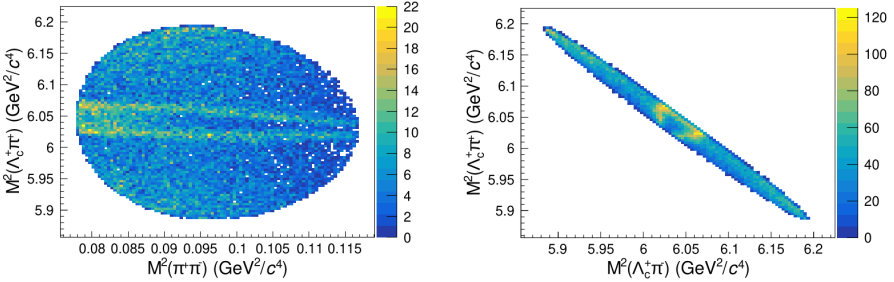

FIG. 2: Dalitz plot for $\Lambda_c(2625)^+$ candidates in the signal region. Explanations of the patterns in the text.

Clear $\Sigma_c(2455)^{++}$ and a reflection of Σ_c^0 in $\Lambda_c^+\pi^+$.

Tiny excess due to $\Sigma_c(2520)$ at the top.

Projections of Dalitz plot fit

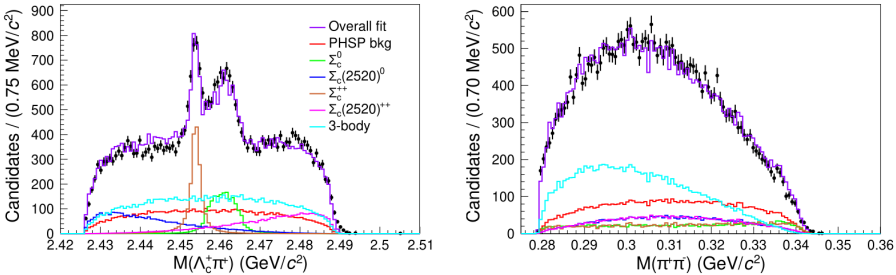

FIG. 3: Dalitz plot fit result plotted as projections. Solid lines shows the overall fitted distribution and its individual components as indicated in the legend. More explanations in the text.

Clear $\Sigma_c(2455)^{++}$ and a reflection of Σ_c^0 in $\Lambda_c^+\pi^+$, again.

Small $\Sigma_c(2520)$ on the sides in $\Lambda_c^+\pi^+$. $\Lambda_c^+\pi^+\pi^-$ is asymm. while bkg. is simm. in $\pi^+\pi^-$.

Yields of $\Lambda_c(2625)^+$, $\Sigma_c(2455)^{++}$, $\Sigma_c(2455)^0$ obtained. Not all $\Sigma_c(2455)$ come from $\Lambda_c(2625)^+$.

Dalitz plot fits of $\Lambda_c(2625)^+$ sidebands

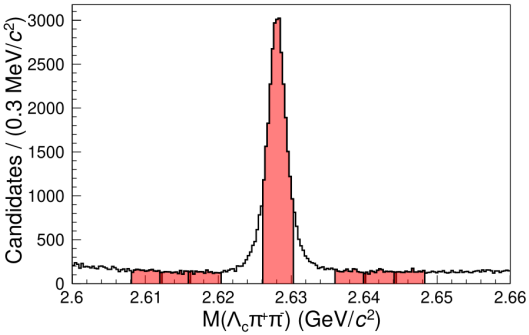

FIG. 4: Signal region and the six sideband regions on either side of the signal region used for sideband subtraction.

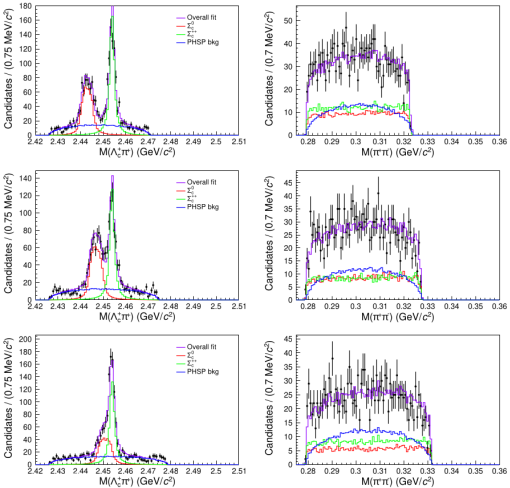

FIG. 5: Projections of the Dalitz plot fits of the 3 sidebands on the left side of the signal region. Overall fitted distribution and the individual fitted components are shown alongside the experimental data.

$\Sigma_c(2455)$ yields extrapolation from $\Lambda_c(2625)^+$ sidebands

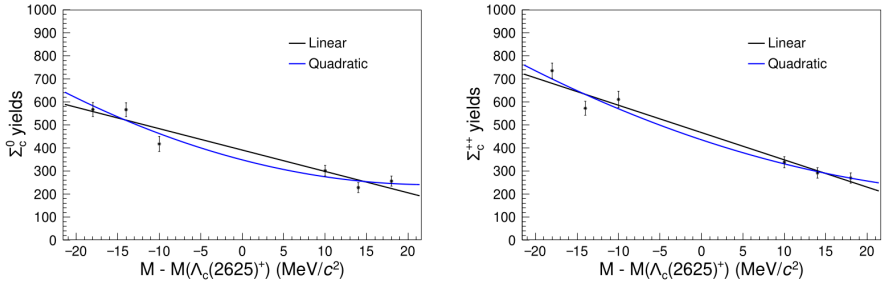

FIG. 7: Σ_c^0 and Σ_c^{++} yields from the sideband Dalitz plot fits, overlaid with linear and quadratic extrapolations.

$$\frac{\mathcal{B}(\Lambda_c(2625)^+ \to \Sigma_c^0\pi^+)}{\mathcal{B}(\Lambda_c(2625)^+ \to \Lambda_c^+\pi^+\pi^-)} = (5.19 \pm 0.23)\%$$

$$\frac{\mathcal{B}(\Lambda_c(2625)^+ \to \Sigma_c^{++}\pi^-)}{\mathcal{B}(\Lambda_c(2625)^+ \to \Lambda_c^+\pi^+\pi^-)} = (5.13 \pm 0.26)\%$$

Systematic uncertainties of the $\Lambda_c(2625)^+$ measurement

$\Lambda_c(2625)^+$ mass precision is limited by Belle capabilities.

- Based on D^{*+} decays, soft pions are calibrated so that $m_{D^{*+}}$ matches the world average.
- Applying this calibration to $\Lambda_c(2625)^+$ shifts its mass.
- Belle also corrects low momenta, which slightly affects the mass measurement.

$\Lambda_c(2625)^+$ branching ratios uncertainties come from

- $\Lambda_c(2625)^+$ yield itself, $\Sigma_c(2455)^{++}$ and $\Sigma_c(2455)^0$ yields and bkg. corrections.
- $\Lambda_c(2625)^+$ yield is most affected by the mass resolution.
- Masses and widths of $\Sigma_c(2455)$ are varied within world average errors.
- Linear or quadratic extrapolation for $\Sigma_c(2455)$ yield corrections.
- The finite MC sample size is also a source.

$\Lambda_c(2625)^+$ measurement results

- $\Lambda_c(2625)^+$ mass measurement is the most precise yet and is consistent with previous ones

$$m_{\Lambda_c(2625)^+} = 2627.978 \pm 0.006 \pm 0.049 \text{ MeV}$$

- $\Lambda_c(2625)^+$ width upper limit is the smallest yet

$$\Gamma_{\Lambda_c(2625)^+} < 0.52 \text{ at } 90\% \text{ C.L.}$$

  Some predictions are ruled out, but higher precision is required.

- $\Lambda_c(2625)^+$ branching ratios extracted from a full Dalitz plot fit are their first measurements

$$\frac{\mathcal{B}\left(\Lambda_c(2625)^+ \to \Sigma_c(2455)^0\pi^+\right)}{\mathcal{B}\left(\Lambda_c(2625)^+ \to \Lambda_c^+\pi^+\pi^-\right)} = (5.19 \pm 0.23 \pm 0.40)\%$$

$$\frac{\mathcal{B}\left(\Lambda_c(2625)^+ \to \Sigma_c(2455)^{++}\pi^-\right)}{\mathcal{B}\left(\Lambda_c(2625)^+ \to \Lambda_c^+\pi^+\pi^-\right)} = (5.13 \pm 0.26 \pm 0.32)\%$$